Thin-Film $Cu_{1-x}N_x$ Catalysts for efficient CO_2 Reduction: A Scalable Magnetron Sputtering Approach

Supporting Information

Mathias van der Veer[a,b], Nick Daems[a], Pegie Cool[b], and Tom Breugelmans[a]

[a] Applied Electrochemistry and Catalysis (ELCAT), University of Antwerp, Campus Drie Eiken, Universiteitsplein 1, 2610 Wilrijk, Belgium

[b] Laboratory of Adsorption and Catalysis (LADCA), University of Antwerp, Campus Drie Eiken, Universiteitsplein 1, 2610 Wilrijk, Belgium

Table of contents

Experimental methods

Experimental methods

Physico-chemical characterization

Various $Cu_{1-x}N_x$ films were deposited by reactive magnetron DC sputtering (Moorfield Lab125) on gas diffusion electrodes (GDE, Sigracet 39BB) utilizing a Cu target (Purity: 99.9999%), argon (Ar) as inert sputtering gas, nitrogen (N_2) as reactive gas, and a substrate capable of sputtering up to 800 cm^2, allowing for scalable synthesis of electrodes with low loadings < 500 µg cm^{-2}. Prior to sputtering, the chamber was evacuated to a vacuum level of less than 9 x 10^{-6} µbar, subsequently the Cu target was cleaned for 2 minutes with argon, without exposing the substrate. The deposition unit (Infinicon SQC-310C) regulates various parameters, such as the operational pressure (P), which was varied between 6 – 10.5 – 15 µbar, furthermore, the r_{N2} factor ($r_{N2} = \frac{N_2}{N_2 + Ar}$) was changed in steps of 0 – 0.25 – 0.5 – 0.75, by varying the gas flow rates. The thickness of the r_{N2} = 0 sample was controlled at 400 nm, as per our previous work where this was the optimal Cu thickness for the eCO_2R.[1] The thickness range of across all samples is estimated to be from 250 to 400 nm, and the degree of variation due to local thickness variations is ± 30 nm.

Finally, the deposition unit allows us to control the sputter rate on the Cu target and is linked with a proportional and automatic change in the required power density, so we set the sputter rate between 1Å s^{-1} - 10Å s^{-1} in steps of 3, and the needed power density was automatically adjusted by the deposition unit. The deposition process involved rotating the substrate at 10 rpm; the temperature was maintained at 20°C with a deposition time of 15 min. The distance between substrate and Cu target was 80 mm. A summary of the deposition conditions is provided in Table S1.

ICP – MS analysis was performed on a 0.28 cm^2 circular sample cut from the catalyst coated GDE, which was submerged in 1 mL of nitric acid (TraceSELECT^{tm}, >69.0%) at 70 °C, and kept overnight. This will dissolve all of the copper that was on the carbon substrate into the solution. Afterwards, we take out the carbon substrate and further dilute the resulting solution containing all the originally deposited copper with MQ before analysing it with ICP – MS. Eventually, we obtain a total µg of Cu that is present in solution, and dividing this with the area of the sample (0.28 cm^2) gives an indication of the pure Cu loading in µg cm^{-2}. The structural characteristics were analyzed using X – ray diffraction (XRD) with Cu Kα radiation on a Bruker D8 ECO diffractometer, covering a range of 20 – 60° 2θ. The SEM – EDX measurements were performed using a Thermo Fischer Scientific Quanta FEG 50 microscope equipped with an ETD detector operated at an accelerated voltage of 20 kV. Contact angle measurements, representative of the hydrophobicity of the material, were performed on an OCA 15EC from Dataphysics. Typically, a 5 µL droplet of water was deposited onto the GDE, and the inner angle formed between the droplet and the surface was measured as an indication of hydrophobicity.

Electrochemical characterization

The electrochemical active surface area (EASA) was determined by the double-layer capacitance (C_{dl}) method, and cyclic voltametric measurements were taken around the Open Circuit Potential (OCP, ± 50 mV) at different scan rates (25 – 50 – 75 – 100 – 125 mV s^{-1}). From the corresponding current vs. scan rate plots, C_{dl} was estimated This value is an estimation of the overall roughness of the thin film, a higher value results in more active sites that are exposed, which indicates that the surface has a more rough structure.

Evaluation of the electrochemical CO_2 reduction reaction (eCO_2R) of the various $Cu_{1-x}N_x$ films was performed using an in-house developed flow electrolyzer as displayed in Figure S1. The working electrode (2 cm^2) rests on an interdigitated designed graphite plate and consists of the prepared GDE samples, with electrical contact on the backside of the graphite plates (for cathode and anode) provided

via a copper current collector, as described previously.[2] Ag/AgCl (sat. KCl) was used as the reference electrode, to control the cathodic potential, and a nickel foam as the counter electrode. Chronopotentiometric electrolysis was performed using high purity CO_2 (99.996%), which was continuously fed through the electrolyzer at a rate of 15 sccm by a mass flow controller. The cathodic and anodic chamber were separated by a Nafion® 117 membrane. The anolyte, 2 M KOH, was recycled over the Ni foam at a flow rate of 2.6 mL min^{-1}. The catholyte stream, i.e. 0.5 M $KHCO_3$ (pH ≈ 8.5), was circulated (single – pass) through the cathodic chamber at a flow rate of 2.6 mL min^{-1}. All experiments were repeated three times for reproducibility and with a current density of – 150 mA cm^{-2}.

An in – line GC measured the formation of various gaseous products such as hydrogen (H_2), carbon monoxide (CO), methane (CH_4), and ethylene (C_2H_4), a flow meter was placed before the GC inlet so that the correct flow (sccm) was used in the calculations. Simultaneously, a liquid sample from the outgoing catholyte was collected for subsequent off-line analysis with GC – FID and HPLC for the detection of alcohols, acetic, and formic acid. For the alcohols, a mixture of standard solutions (1000 ppm) was prepared for ethanol (C_2H_5OH), propanol (C_3H_7OH), and allyl alcohol (C_3H_5OH), 100 µL of each standard mixed with 100 µL of butanol (internal standard), and 600 µL of MQ water and the vials were vortexed to assure an optimal, homogenous solution. The measured samples were prepared by adding 100 µL of butanol to 900 µL sample and they were vortexed again prior to analysis. The HPLC was used for the detection of acetate (CH_3COO^-) and formate ($HCOO^-$), and samples were prepared by filtrating 900 µL of liquid product with 900 µL $HClO_4$ (1.2 M) to precipitate the catholyte salts, the resulting liquid was collected in a vial and analyzed together with a formic acid standard of 1000 ppm. The quantification allows us to calculate the faradaic efficiency (FE) based on the measured ppm and the cathodic energy efficiency (cEE),

Finally, to evaluate the catalytic performance, faradaic efficiencies (FEs) of the liquid and gaseous products were determined according to the following equations:

$$FE\% = 100 * \frac{n * F * C * V}{Q} \quad \text{(Eq. 1)}$$

$$FE\% = 100 * \frac{n * F * C * v * P}{R * T * l} \quad \text{(Eq. 2)}$$

Here, n represents the number of electrons exchanged, F the faraday constant 96485 A*s mol^{-1}, C denotes the concentration of the product, V the amount of electrolyte, Q the charge given in A s, v the gas flow rate in mL min^{-1}, P = 101.325 kPa, R = 8.314 J $(mol\ K)^{-1}$, T = 298 K and l the applied current (A).

$$EE\% = 100 * \frac{FE * E_{theoretical}}{E_{experimental}} \quad \text{(Eq. 3)}$$

The cathodic energy efficiency (EE) is a metric of energy input, which takes into account the difference in theoretical and observed potential. $E_{theoretical}$ is the difference of the water oxidation potential (1.23 V vs RHE) and the standard reduction potential of CO_2 → C_2H_4 (0.065 V vs RHE) or CO_2 → C_2H_5OH (0.085 V vs RHE). The $E_{experimental}$ is the difference between the water oxidation potential and the measured cathodic overpotential. We believe that comparing EE with potentials that are not iR corrected provide a more accurate representation of the actual EE as the ohmic drops is dependent on system configuration. Systems that have large ohmic drops, and where electrolyte conductivity changes over time and is dependent on current density, reduces the accuracy of the iR-correction.[3] Unless continuous iR measurement and compensation is applied, an accurate reading of electrode potential during operation can not be achieved, due to continuous changes to the resistance, which is another reason why we opted not to perform iR correction.[4]

All measured potentials were converted to the reversible hydrogen electrode (RHE) scale according to the Nernst equation shown in Eq.4: where 0.199 V corresponds to the value relative to the standard reduction potential of Ag/AgCl (sat. KCl) for the calculation of EE.

$$E\ (RHE) = E\left(\frac{Ag}{AgCl}\right) + 0.199\ V + 0.059 * pH \quad \text{(Eq. 4)}$$

Table S1. Overview of the different fabricated $Cu_{1-x}N_x$ films along with the measured Cu loading via ICP – MS

Sample	*Ar flow (sccm)*	*N_2 flow (sccm)*	*P (μbar)*	*Rate (Å s^{-1})*	*Cu loading (μg cm^{-2})*	*Power density (W cm^{-2})*	*EDX N%*
r = 0	1	0	6	4	**340**	2.35	0
r = 0.25	3	1	6	4	**307**	2.71	11.2
r = 0.5	1	1	6	4	**288**	2.96	16.3
r = 0.75	1	3	6	4	**267**	3.21	20.8
P = 6	1	1	6	4	**288**	2.96	16.3
P = 10.5	1	1	10.5	4	**276**	3.08	14.7
P = 15	1	1	15	4	**274**	3.33	12.9
SR = 1	1	1	6	1	**194**	2.71	16.1
SR = 4	1	1	6	4	**288**	2.96	16.3
SR = 7	1	1	6	7	**327**	3.21	16.2
SR = 10	1	1	6	10	**411**	3.45	16.5

Table S2. Reported Cu – based catalysts for the eCO_2R to C_{2+} (i.e. ethylene and ethanol), in terms of current density, potential, cell configuration, FE, and EE.'*' Marks potentials and EE that are iR corrected.

Catalyst	*Current density* (*mA cm^{-2}*)	*Potential* *RHE (V)*	*Cell*	*FE_{C2H4}* (*%*)	*FE_{EtOH}* (*%*)	*EE_{C2H4}* (*%*)	*EE_{EtOH}* (*%*)	*C_2H_4 Mass activity* (*mA/mg$_{Cu}$*)
Cu_3N-Derived Cu NW[5]	57	-1.0	H-cell	66	8	34.5	4.1	/
Cu_3N NP[6]	60	-0.8	H-cell	61.1	/	35	/	/
Cu on Cu_3N[7]	35	-0.95*	H-cell	39	19	20.8*	9.9*	71.8
Cu_3N NC[8]	95	-1.6	H-cell	60	< 1	24.7	< 1	2.8
EB-Cu[9]	200	-0.7*	Flow	39	/	24.2*	/	229.4
PE-ALD Cu[10]	30	-0.94*	Flow	42.2	23.2	22.7*	12.2*	460
CuCl derived[11]	400	-0.68*	Flow	56	/	34.2*	/	/
Cu_2O NC[2]	150	-1.59	Flow	24	20	9.9	8.1	18
Multi-grain Cu_2O[12]	800	-0.85*	Flow	46	22	25.8*	12.1*	460
CuO_x [13]	300	-1.15*	Flow	56	16	27.4*	7.7*	916.7
B-$CuZn_{2.5}$[14]	200	-0.45*	Flow	49	22	34*	15*	196
CuAg-ED[15]	300	-0.7*	Flow	60	25	36.2*	14.8*	90
Cu_2O/Ag[16]	900	-1.1*	Flow	23.3	46.3	11.7*	22.8*	65
Pd-Cu-B[17]	300	-1.7	Flow	17.5	35	7	13.7	25.7
$Cu_{99}Ag_1$ thin film[1]	150	-1.73	Flow	42.0	24.2	16.5	9.4	180
Cu_3Sn[18]	900	-3	MEA	/	40	/	17	120
Cu_2O-SiO_2-NH_2[19]	300	-1.7	Flow	40.2	29	16	11.3	120.6
Cu_2O/CuO[20]	250	-4.2	MEA	40	20.8	8.6	4.4	200
CuZn/$CuZnAlO_2O_4$[21]	400	-1.15	Flow	36	36.3	17.6	17.3	144
$Cu_{0.84}N_{0.16}$ Thin Film	**150**	**-1.35**	**Flow**	**44.2**	**21.6**	**20**	**9.6**	**230.2**
$Cu_{0.84}N_{0.16}$ Thin Film	**150**	**-0.633***	**Flow**	**44.2**	**21.6**	**27.6***	**13.3***	**230.2**

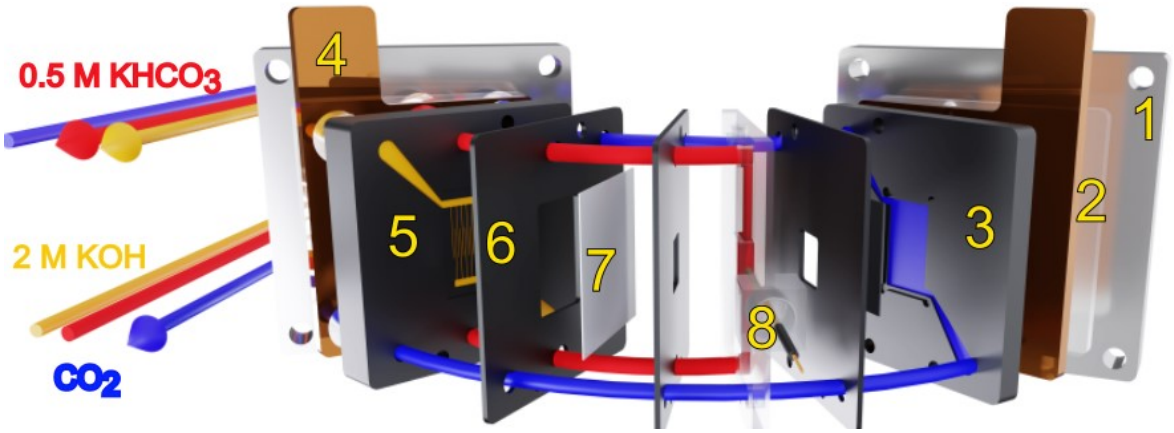

Figure S1. View of in-house developed flow electrolyzer; (1) Aluminum backplate, (2) PMMA isolation plates, (3) Cathode flat graphite plate with GDE, (4) conductive copper plates, (5) Anode graphite plate with Nickel foam, (6) EPDM gaskets to seal, (7) Nafion 117 membrane, (8) Reference electrode chamber with Ag/AgCl. Flow channels for gaseous CO_2, catholyte, and anolyte.

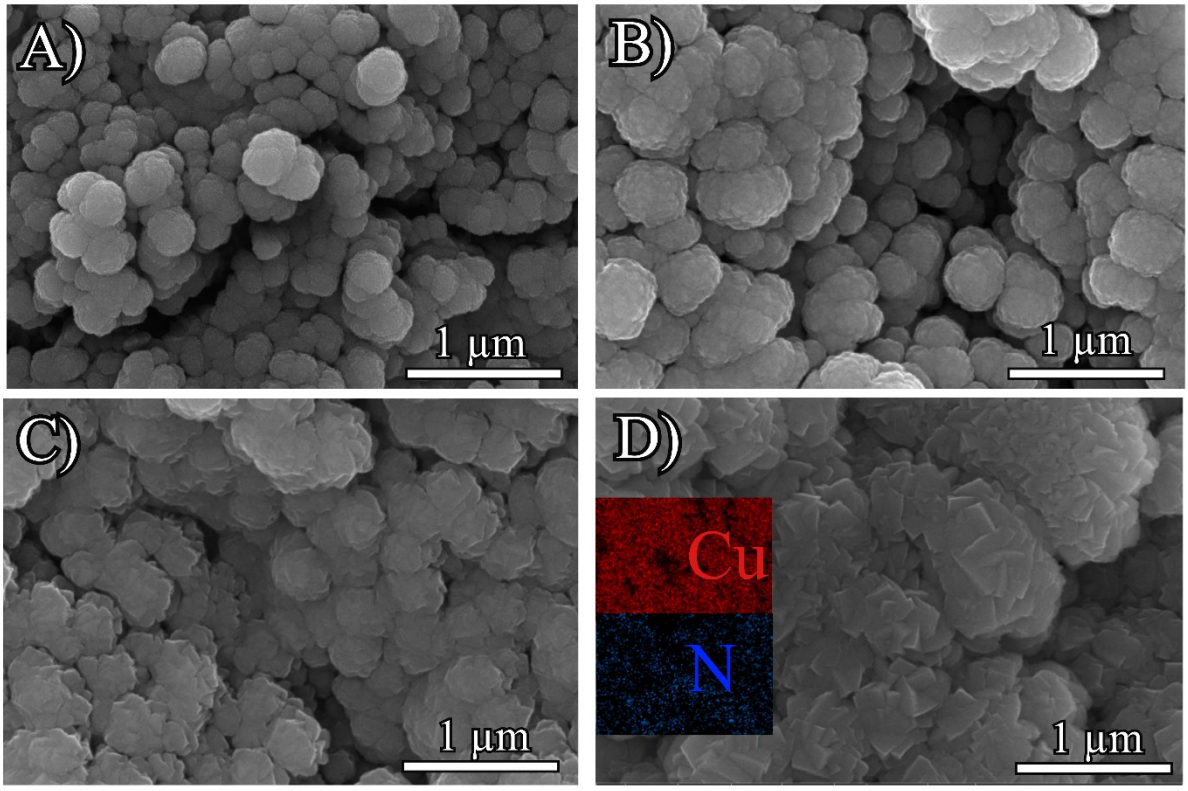

Figure S2.SEM images at 1 µm scale magnification of $Cu_{1-x}N_x$ films prepared with an operational pressure of 6 µbar and a sputter rate of 4 Å s^{-1}, for different r_{N2} ratios, A) $r_{N2} = 0$, B) $r_{N2} = 0.25$, C) $r_{N2} = 0.50$, and D) $r_{N2} = 0.75$

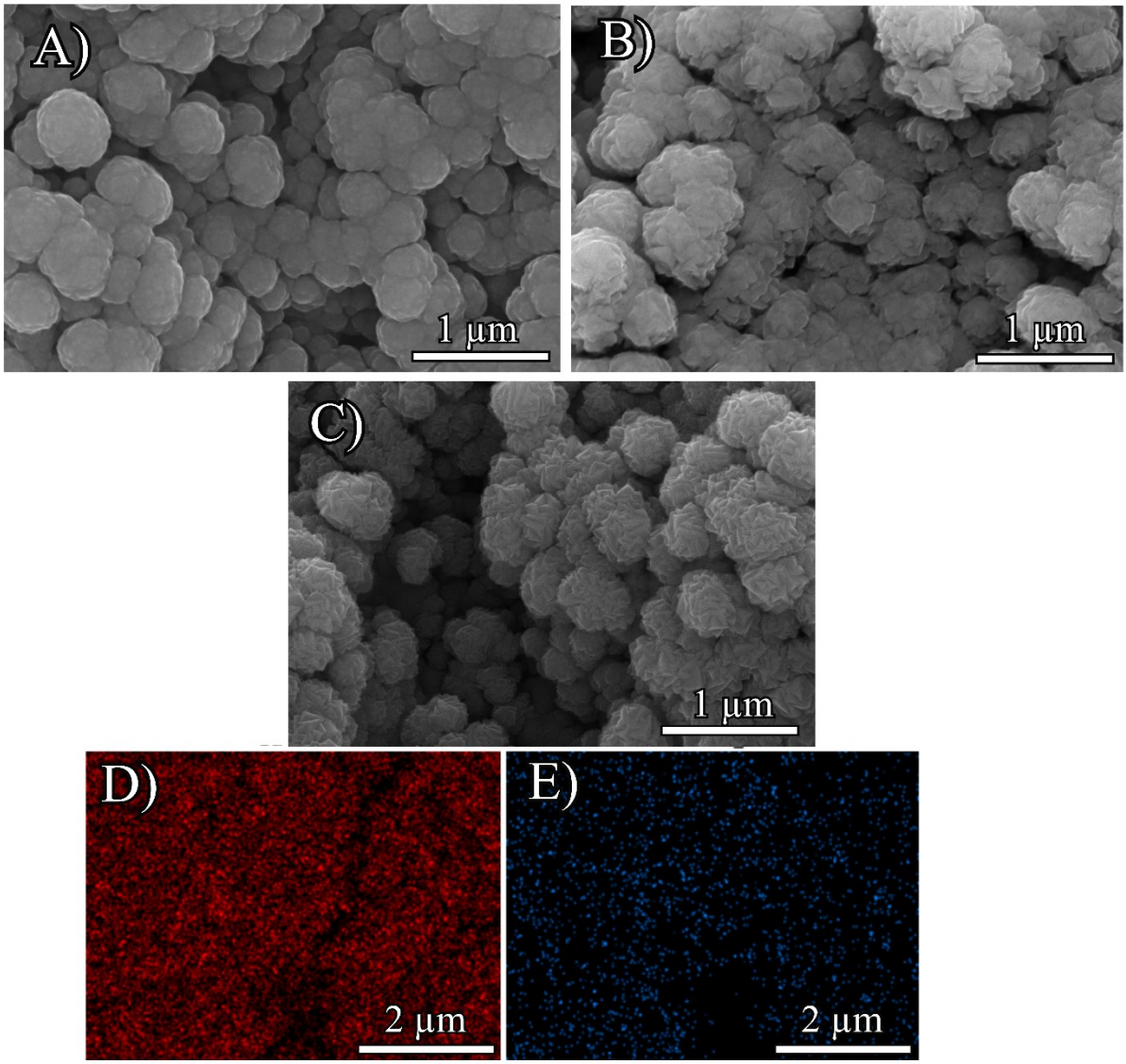

Figure S3. SEM images at 1 µm scale magnification of $Cu_{1-x}N_x$ films prepared with a r_{N2} factor of 0.50, and a sputter rate of 4 Å s^{-1}, for different operational pressures, A) P = 6 µbar, B) P = 10.5 µbar, C) P = 15 µbar. EDX maps of D) Cu, and E) N.

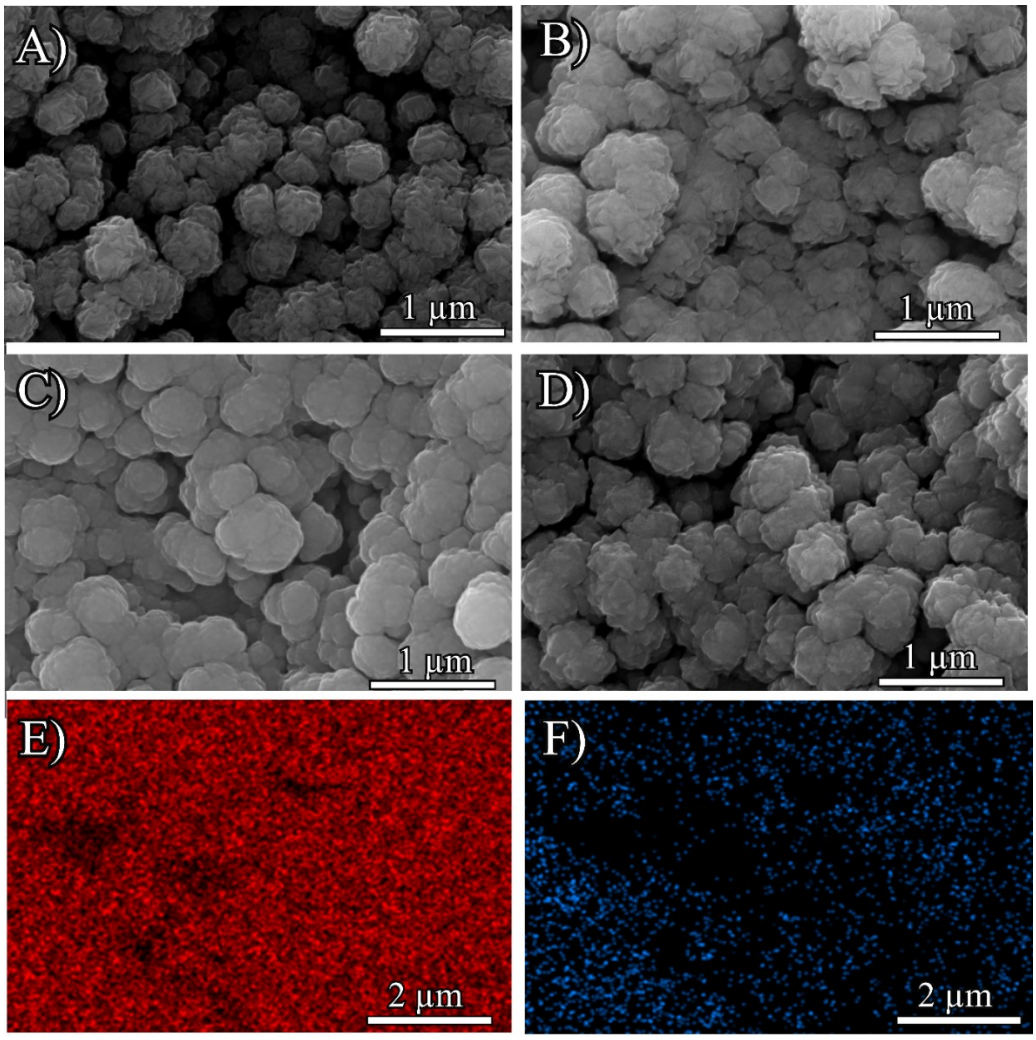

Figure S4. SEM images at 1 µm scale magnification of $Cu_{1-x}N_x$ films prepared with a r_{N2} factor of 0.50, and an operational pressure of 6 µbar, for different SR rates, A) SR = 1 Å/s, B) SR = 4 Å/s, C) SR = 7 Å/s, and D) SR = 10 Å/s. EDX maps of E) Cu, and F) N.

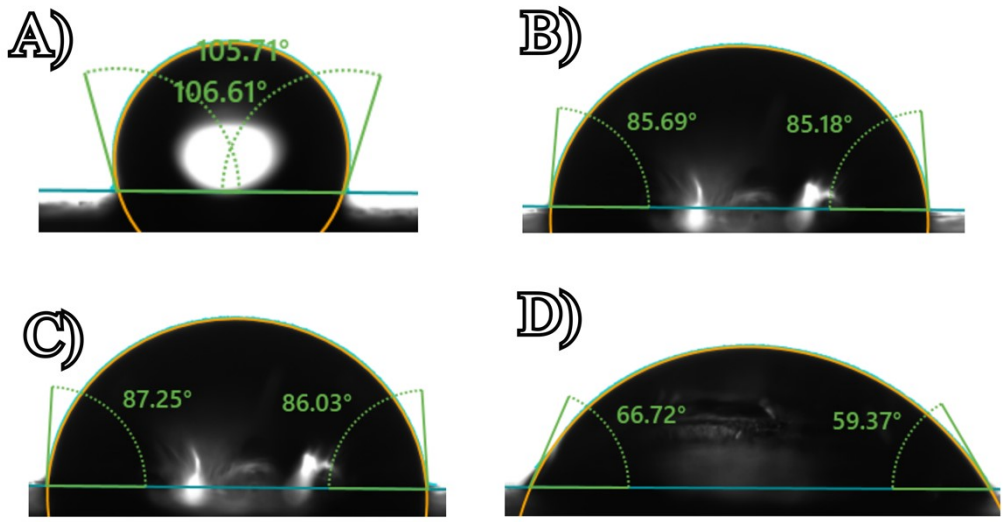

Figure S5. Contact angle measured on $Cu_{1-x}N_x$ films prepared with an operational pressure of 6 µbar and a sputter rate of 4 Å s^{-1}, for different r_{N2} ratios, A) $r_{N2} = 0$, B) $r_{N2} = 0.25$, C) $r_{N2} = 0.50$, and D) $r_{N2} = 0.75$.

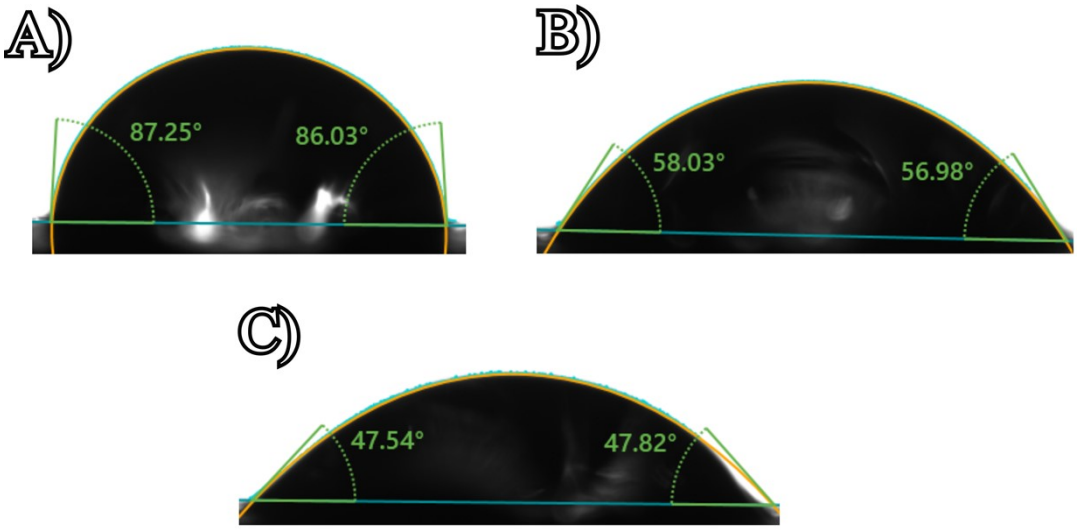

Figure S6. Contact angle measured on $Cu_{1-x}N_x$ films prepared with a r_{N2} factor of 0.50, and a sputter rate of 4 Å s^{-1}, for different operational pressures, A) P = 6 µbar, B) P = 10.5 µbar, C) P = 15 µbar.

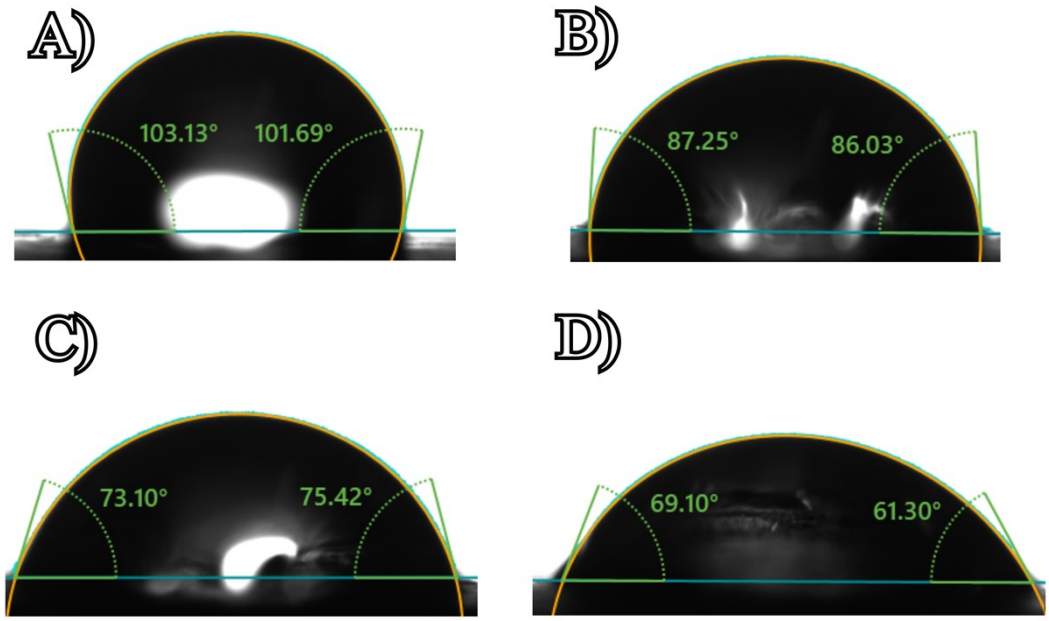

Figure S7. Contact angle measured on $Cu_{1-x}N_x$ films prepared with a r_{N2} factor of 0.50, and an operational pressure of 6 μbar, for different SR ratios, A) SR = 1 Å s^{-1}, B) SR = 4 Å s^{-1}, C) SR = 7 Å s^{-1}, and D) SR = 10 Å s^{-1}.

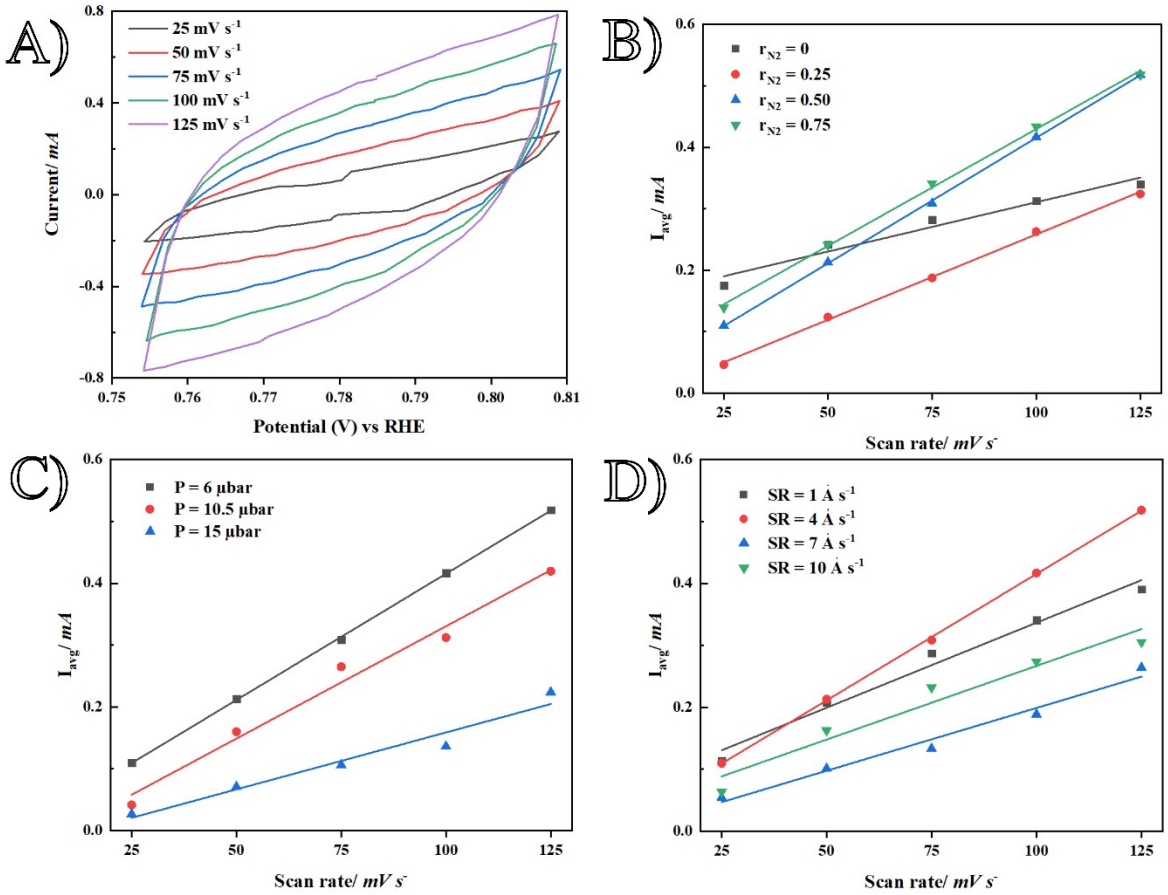

Figure S8. A) Cyclic voltammograms taken with r_{N2} = 0.50 around OCP with different scan rates of 25; 50; 75; 100; 125 mV s^{-1}. B) Linear fit between average current at OCP vs scan rate for $Cu_{1-x}N_x$ films prepared with different r_{N2} values of 0; 0.25; 0.50; 0.75. C) Linear fit between average current at OCP vs scan rate for $Cu_{1-x}N_x$ films prepared with different pressures of 6; 10.5; 15 µbar. D) Linear fit between average current at OCP vs scan rate for $Cu_{1-x}N_x$ films prepared with different SR values of 1; 4; 7; 10 Å s^{-1}.

Table S3. For every prepared $Cu_{1-x}N_x$ films with different operational parameters, the potential at 1 hour along with the calculated EE for ethylene and ethanol, and finally the C_{dl} value.

Catalyst	*Potential V vs RHE*	*EE_{C2H4} (%)*	*EE_{EtOH} (%)*	*C_{dl} (mF)*
r_{N2} = 0	-2.04	15.6	7.9	1.61
r_{N2} = 0.25	-1.52	18.64	8.1	2.78
r_{N2} = 0.5	**-1.35**	**20**	**9.6**	**4.08**
r_{N2} = 0.75	-1.45	19.2	8.4	3.8
P = 6	**-1.35**	**20**	**9.6**	**4.08**
P = 10.5	-1.95	13.6	8.2	3.63
P = 15	-2.05	13.7	6.7	1.84
SR = 1	-2.09	15.1	6.5	2.75
SR = 4	**-1.35**	**20**	**9.6**	**4.08**
SR = 7	-1.61	17.9	8.4	2.03
SR = 10	-2.68	11.8	5.8	2.38

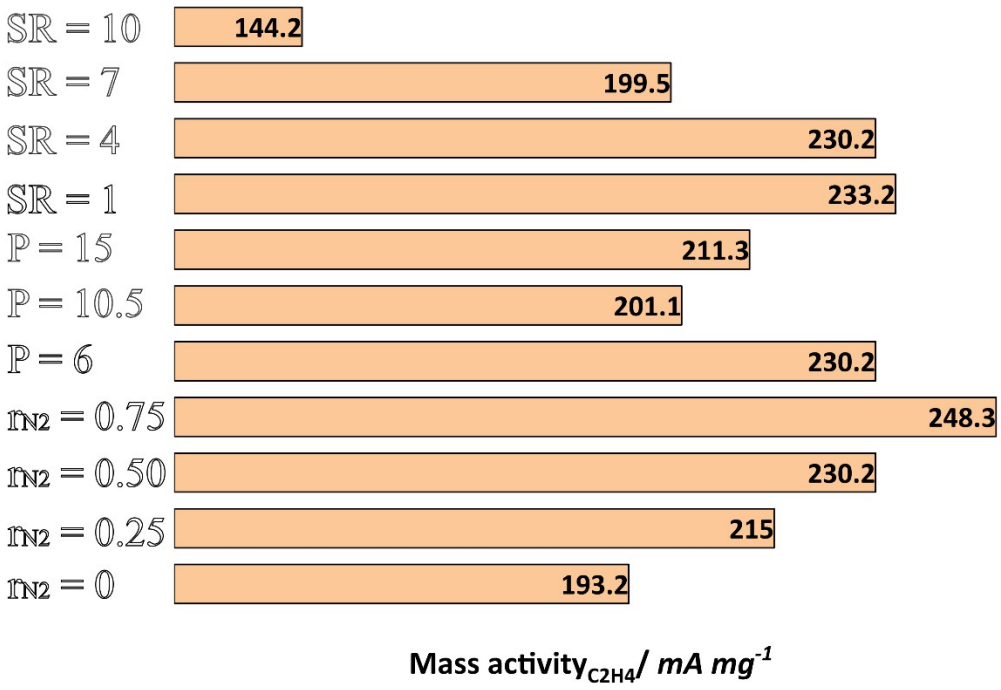

Figure S9. $Cu_{1-x}N_x$ films prepared with different operational parameters, and the calculated partial mass activity for ethylene based on the Cu loading and FE_{C2H4}.

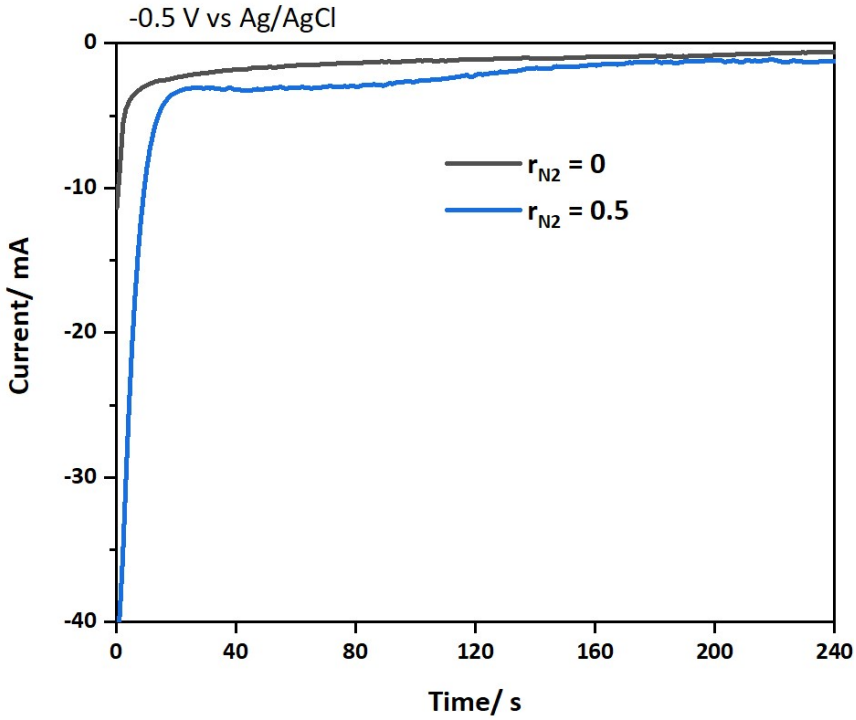

Figure S10. Chronoamperometry run at – 0.5 V vs Ag/AgCl, in a batch cell with Ar - saturated - 1 M K_2SO_4 as electrolyte, Ni foam as counter electrode, and a Ag/AgCl reference electrode, for r_{N2} = 0, and r_{N2} = 0.5. Integrating the area above the curves gives the total coulombs.

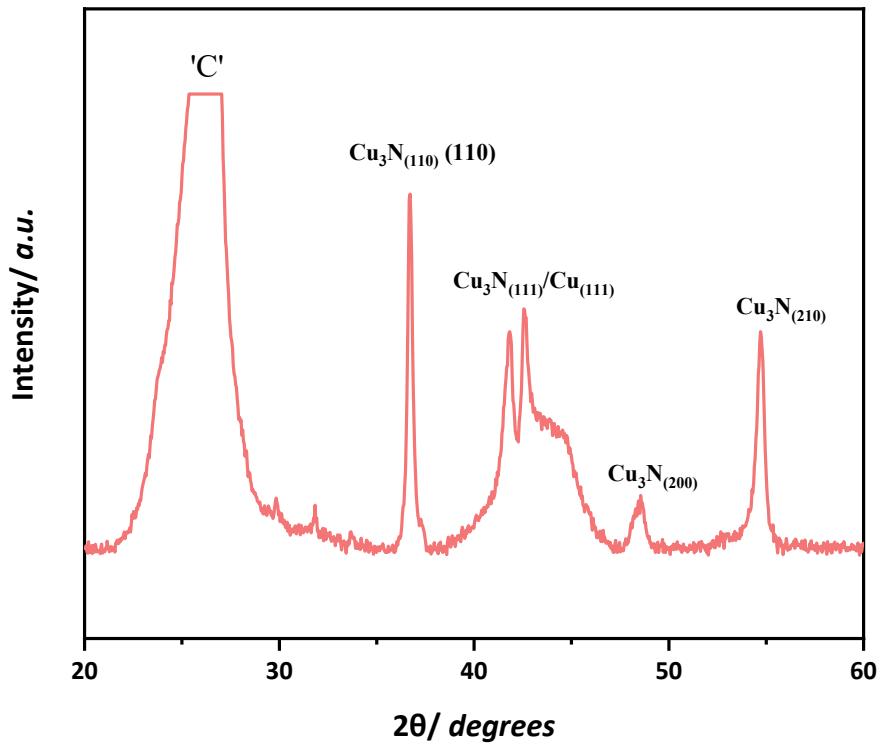

Figure S11. XRD pattern of the spent $Cu_{0.84}N_{0.16}$ sample prepared with $r_{N2} = 0.50$, operational pressure of 6 μbar, and sputter rate of 4 Å s^{-1}, with indicated phases and hkl indices.

1. Veer, M. van der, Daems, N., Cool, P. & Breugelmans, T. Enhancing selectivity and stability in electrochemical CO2 reduction using tailored sputtered CuAg electrodes. *Green Chemistry* (2025) doi:10.1039/D4GC06164K.

2. van der Veer, M., Daems, N., Cool, P. & Breugelmans, T. From batch to flow: the effect of pH, current, and the crystal facets of Cu2O on electrochemical CO2 reduction. *Sustain Energy Fuels* **8**, 2504–2518 (2024).

3. Sassenburg, M. *et al.* Characterizing CO2 Reduction Catalysts on Gas Diffusion Electrodes: Comparing Activity, Selectivity, and Stability of Transition Metal Catalysts. *ACS Appl Energy Mater* **5**, 5983–5994 (2022).

4. Heenan, A. R., Hamonnet, J. & Marshall, A. T. Why Careful iR Compensation and Reporting of Electrode Potentials Are Critical for the CO2Reduction Reaction. *ACS Energy Lett* **7**, 2357–2361 (2022).

5. Mi, Y. *et al.* Selective Electroreduction of CO 2 to C2 Products over Cu 3 N-Derived Cu Nanowires. *ChemElectroChem* **6**, 2393–2397 (2019).

6. Wang, H. *et al.* Cu3N nanoparticles with both (100) and (111) facets for enhancing the selectivity and activity of CO2 electroreduction to ethylene. *New Journal of Chemistry* **46**, 12523–12529 (2022).

7. Liang, Z. Q. *et al.* Copper-on-nitride enhances the stable electrosynthesis of multi-carbon products from CO2. *Nature Communications 2018 9:1* **9**, 1–8 (2018).

8. Yin, Z. *et al.* Cu3n nanocubes for selective electrochemical reduction of co2 to ethylene. *Nano Lett* **19**, 8658–8663 (2019).

9. Jiao, F. *et al.* Scalable gas diffusion electrode fabrication for electrochemical CO2 reduction using physical vapor deposition methods. *ACS Appl Mater Interfaces* **14**, 7731–7740 (2022).

10. Lenef, J. D. *et al.* Atomic Layer Deposition of Cu Electrocatalysts on Gas Diffusion Electrodes for CO2 Reduction. *Nano Lett* **23**, 10779–10787 (2023).

11. Golam Kibria, M. *et al.* A Surface Reconstruction Route to High Productivity and Selectivity in CO2 Electroreduction toward C2+ Hydrocarbons. *Advanced Materials* **30**, 1804867 (2018).

12. Lv, X. *et al.* Grain refining enables mixed Cu+/Cu0 states for CO2 electroreduction to C2+ products at high current density. *Appl Catal B* **324**, (2023).

13. Daems, N. *et al.* Steering Hydrocarbon Selectivity in CO2 Electroreduction over Soft-Landed CuOx Nanoparticle-Functionalized Gas Diffusion Electrodes. *ACS Appl Mater Interfaces* **14**, 2691–2702 (2022).

14. Song, Y. *et al.* B-Cu-Zn Gas Diffusion Electrodes for CO2 Electroreduction to C2+ Products at High Current Densities. *Angewandte Chemie International Edition* **60**, 9135–9141 (2021).

15. Hoang, T. T. H. *et al.* Nanoporous Copper-Silver Alloys by Additive-Controlled Electrodeposition for the Selective Electroreduction of CO2 to Ethylene and Ethanol. *J Am Chem Soc* **140**, 5791–5797 (2018).

16. Wu, X. *et al.* Pulsed Electrolysis Promotes CO2 Reduction to Ethanol on Heterostructured Cu2O/Ag Catalysts. *Small* **20**, 2307637 (2024).

17. Bagchi, D. *et al.* Operando Investigation of the Origin of C─C Coupling in Electrochemical CO2 Reduction Upon Releasing Bonding Strength, Structural Ordering in Pd─Cu Catalyst. *Adv Energy Mater* **14**, 2402237 (2024).

18. Shang, L., Lv, X., Zhong, L., Li, S. & Zheng, G. Efficient CO2 Electroreduction to Ethanol by Cu3Sn Catalyst. *Small Methods* **6**, 2101334 (2022).

19. Zhang, Z. Y. *et al.* SiO 2 assisted Cu 0 –Cu + –NH 2 composite interfaces for efficient CO 2 electroreduction to C 2+ products. *J Mater Chem A Mater* **12**, 1218–1232 (2024).

20. Shi, H. *et al.* Stabilizing Cu+ Species in Cu2O/CuO Catalyst via Carbon Intermediate Confinement for Selective CO2RR. *Adv Funct Mater* **34**, 2310913 (2024).

21. Zhang, Z. Y. *et al.* Cu-Zn-based alloy/oxide interfaces for enhanced electroreduction of CO2 to C2+ products. *Journal of Energy Chemistry* **83**, 90–97 (2023).